

Role of 2p-2h MEC excitations in superscaling

A. De Pace,¹ M. Nardi,¹ W. M. Alberico,¹ T. W. Donnelly,² and A. Molinari¹

¹*Istituto Nazionale di Fisica Nucleare,*

Sezione di Torino and Dipartimento di Fisica Teorica,

via Giuria 1, I-10125 Torino, Italy

²*Center for Theoretical Physics, Laboratory for Nuclear Science and Department of Physics,
Massachusetts Institute of Technology, Cambridge, MA 02139, USA*

Abstract

Following recent studies of inclusive electron scattering from nuclei at high energies which focused on two-nucleon emission mediated by meson-exchange currents, in this work the superscaling behavior of such contributions is investigated. Comparisons are made with existing data below the quasielastic peak where at high momentum transfers scaling of the second kind is known to be excellent and scaling of the first kind is good, in the proximity of the peak where both 1p-1h and 2p-2h contributions come into play, and above the peak where inelasticity becomes important and one finds scaling violations of the two kinds.

PACS numbers: 25.30.Rw, 25.30.Fj, 24.30.Gd, 24.10.Jv

Keywords: scaling; relativistic electromagnetic nuclear response; 2p-2h meson exchange currents; Δ resonance

I. INTRODUCTION

The superscaling behavior of the nuclear inclusive semi-leptonic electroweak response in the quasielastic (QE) region has been seen to be a useful concept, as illustrated and discussed in recent work [1, 2, 3]. Superscaling stands for scaling both in the three-momentum $q \equiv |\mathbf{q}|$ transferred from the probe to the nucleus (scaling of the first kind, often referred to as y -scaling) and in a momentum that is characteristic of a given nucleus (scaling of the second kind). The latter characteristic parameter is often taken for simplicity to be the Fermi momentum k_F , and hence equivalently scaling of the second kind is related to the density ($\propto k_F^3$) of a given nuclear species. Of course, the choice of k_F as a scaling variable arises naturally in the Relativistic Fermi Gas (RFG) model which was used initially in Ref. [4] to motivate the introduction of the concept of superscaling.

In particular, in studies of scaling the inclusive cross sections (or, if available, the individual separated responses) are first divided by an appropriate single-nucleon cross section. For example, in electron scattering from a nucleus with charge and neutron numbers Z and N , respectively, the dividing factor has the form $Z\sigma_{ep} + N\sigma_{en}$. For scaling of the first kind one displays this reduced cross section against an appropriately chosen scaling variable, such as the familiar y variable or a dimensionless analog called ψ (or ψ' if a phenomenological energy shift is included; see the discussions in the next section for details), and in some kinematic regimes observes a universality of the results with respect to the choice of momentum transfer. That is, the result scales. Specifically one finds that this behavior occurs when the momentum transfer is sufficiently large (typically larger than about 500-700 MeV/c) and only when the energy transfer is lower than the value that characterizes the position of the quasielastic peak (QEP), the so-called scaling region. In contrast, as emphasized in Refs. [1, 2, 3] and also in Refs. [5, 6], scaling of the second kind proceeds from the same reduced cross section, but now (1) makes the reduced cross section or scaling function dimensionless by multiplying it by the characteristic nuclear momentum scale (called k_F henceforth) and (2) displays this as a function of a dimensionless scaling variable, again scaled by division by k_F . In the scaling region one finds universality for different nuclear species at given kinematics. When both types of scaling occur one says that the response superscales.

In fact, only the longitudinal part of the response appears to superscale (see Ref. [7] and

also [1, 2, 3]), and even in the scaling region one finds some degree of scaling violation which appears to arise in the transverse part of the response. Thus the longitudinal contributions, apparently being essentially impulsive at high energies, are usually used to determine the basic nuclear physics of quasielastic scattering. This leaves us with the transverse contributions to explain. In the region above the QEP it is natural to have scaling violations, since the reaction mechanism there is not solely impulsive knockout of protons and neutrons, but may proceed via meson production including via baryon resonances such as the Δ . One knows that these contributions are much more prominent in the transverse response than in the longitudinal contributions and hence it is reasonable to expect some of the scaling violations to arise this way. But this is not the entire story: even below meson production threshold there are scaling violations in the transverse response. One source for this is expected to be the role played by the Meson-Exchange Current (MEC) contributions, which again are predominantly transverse (see for example Ref. [8]), and this has motivated the present study.

Specifically, in this work we shall present a first exploration of the impact of the two particle–two hole (2p-2h) excitations induced by the MEC on the superscaling behavior of the transverse RFG response. In the present work we limit the scope to MEC contributions mediated by pion exchange and include contributions both from intermediate nucleons and also Δ isobars. Our results are compared with the relevant data to assess the role of such MEC effects in explaining the scale breaking.

In carrying out this task we take advantage of a very recent calculation of the 2p-2h MEC contribution to the RFG transverse response performed fully respecting Lorentz and translational invariance [9]. The same type of analysis of the RFG response has also been carried out in the 1p-1h sector, for both the longitudinal and transverse channels, in a scheme that is not only Lorentz and translational, but gauge invariant as well [10]. In order to fulfill gauge invariance also in the 2p-2h sector of the RFG Hilbert space, an extension to include 2p-2h excitations induced by correlations, in addition to the MEC, is required. This topic is currently under investigation.

In the present paper we start by briefly outlining in Sect. II the formalism that lies at the basis of our study. Next, in Sect. III, we explore the kinematical domain to the left of the QEP (that is, $\psi' \leq 0$), which is dominated, for $\psi' > -1$, by 1p-1h excitations. Past investigations [1, 2, 3] have convincingly demonstrated that for $\psi' \leq 0$ second-kind scaling is

quite well satisfied: indeed, the data scale almost perfectly in k_F if the latter is appropriately chosen¹. Also, at least at sufficiently large values of q , scaling of the first kind appears quite well obeyed by nature for $\psi' \leq 0$, although not as well as scaling of the second kind.

In this work we observe an important contribution of 2p-2h MEC in the kinematical region lying below $\psi' = -1$, where the RFG 1p-1h processes are forbidden. In the region nearer the QEP where the RFG 1p-1h contributions enter for the transverse scaling function one has, on the one hand, both the 1p-1h MEC and correlation contributions [10, 11, 12] which conspire and interfere with the impulsive contributions (the basic RFG responses) to yield a net transverse response that is reduced with respect to the RFG. On the other hand, the 2p-2h MEC contributions add incoherently and tend to compensate the above reduction. See also Refs. [13, 14, 15]. Note that both classes of contributions provide scaling violations.

After exploring the scaling region and the region of the QEP, in Sect. IV we extend our study to the domain $\psi' \geq 0$, focusing on the impact of the 2p-2h excitations on scaling in the resonance region. Here first-kind scaling is well-known to be very badly violated, owing to the role now played by nucleon excitations and meson production, which, as stated above, are largely transverse. On the other hand, in Ref. [16] it is shown that violations of the transverse second-kind scaling behavior are not so large, although they can be as large as 20% in the resonance region. Again we emphasize that in the present work longitudinal scaling is always assumed to be perfect.

In Sect. V we explore the role of the Δ in the 2p-2h MEC contributions relative to effects arising from two-body currents that contain only nucleons and pions. Some flexibility exists in modeling the former via the effective Lagrangian used in the present work and we present results displaying the impact of changing the parameters in the model.

Clearly, part of the story is contained in the present work where the 2p-2h MEC and their impact on the two kinds of scaling is explored; however, naturally the complete story will have to await the ultimate extensions to larger classes of MEC and correlation effects which are presently being pursued. In the Conclusions we address this issue of what is still missing in our analysis of superscaling and indicate what is being done to complete the (highly non-trivial) study. We also briefly summarize our present findings and comment on

¹ It thus appears that this offers a third method, beyond the ones based upon the nuclear density and the width at half-height of the QEP, to extract this crucial parameter of nuclear structure from the data.

their significance and on future perspectives.

II. FORMALISM

In this section we summarize the basic formulas needed in our analysis of the superscaling physics, closely following Refs. [1, 2, 3]. As is well-known, the inclusive cross section for the scattering of electrons from nuclei in the one-photon exchange approximation reads

$$\frac{d^2\sigma}{d\Omega_e d\omega} = \sigma_M [v_L R_L(\kappa, \lambda) + v_T R_T(\kappa, \lambda)], \quad (1)$$

where σ_M is the Mott cross section and $Q^\mu = (\omega, \mathbf{q})$ is the four-momentum transferred by the virtual photon, with ω its energy transfer, \mathbf{q} its three-momentum transfer and $Q^2 = \omega^2 - \mathbf{q}^2$. Equivalently we may use the dimensionless variables $\lambda \equiv \omega/2m_N$ and $\kappa \equiv |\mathbf{q}|/2m_N$, m_N being the nucleon mass. One then has for the square of the four-momentum transfer $|Q^2|/4m_N^2 \equiv \tau = \kappa^2 - \lambda^2$. In Eq. (1) the kinematical factors are given as usual by

$$v_L = \left(\frac{\tau}{\kappa^2}\right)^2 \quad \text{and} \quad v_T = \frac{\tau}{2\kappa^2} + \tan^2 \frac{\theta_e}{2}, \quad (2)$$

θ_e being the electron scattering angle, while R_L (R_T) is the longitudinal (transverse) response function of a nucleus with Z protons and N neutrons.

The scaling function $F(\kappa, \psi)$ is then defined according to

$$F(\kappa, \psi) = \frac{d^2\sigma/d\Omega_e d\omega}{\sigma_M [v_L G_L(\kappa, \lambda) + v_T G_T(\kappa, \lambda)]}, \quad (3)$$

where the dividing factor, namely the single-nucleon electromagnetic cross section, is given in terms of

$$G_L(\kappa, \lambda) = \frac{(\kappa^2/\tau)^2 \left[\tilde{G}_E^2 + \tilde{W}_2 \Delta \right]}{2\kappa [1 + \xi_F(1 + \psi^2)/2]} \quad (4a)$$

and

$$G_T(\kappa, \lambda) = \frac{2\tau \tilde{G}_M^2 + \tilde{W}_2 \Delta}{2\kappa [1 + \xi_F(1 + \psi^2)/2]}, \quad (4b)$$

with

$$\tilde{G}_E^2 \equiv Z G_{E_p}^2 + N G_{E_n}^2 \quad (5a)$$

$$\tilde{G}_M^2 \equiv Z G_{M_p}^2 + N G_{M_n}^2 \quad (5b)$$

and

$$\tilde{W}_2 \equiv \frac{1}{1 + \tau} \left(\tilde{G}_E^2 + \tau \tilde{G}_M^2 \right). \quad (6)$$

In the above the quantity ψ , the scaling variable, naturally emerges from the RFG studies [4]:

$$\psi \equiv \frac{1}{\sqrt{\xi_F}} \frac{\lambda - \tau}{\sqrt{(1 + \lambda)\tau + \kappa\sqrt{\tau(\tau + 1)}}}, \quad (7)$$

where $\xi_F \equiv \sqrt{1 + \eta_F^2} - 1$ is the Fermi kinetic energy in dimensionless units ($\eta_F \equiv k_F/m_N$). Any independent pair of quantities may be used as kinematics variables, (q, ω) , (Q^2, ω) , (κ, λ) , (q, ψ) , etc., as these are all functionally related. In studies of QE scaling the last choice proves useful and in this work we continue to employ this pair. Moreover, one finds that a small phenomenological energy shift improves the modeling and accordingly we shift $\omega \rightarrow \omega - E_{\text{shift}} \equiv \omega'$ and correspondingly $\lambda \rightarrow \lambda'$ and, by substitution of λ' for λ in Eq. (7), likewise a shifted scaling variable ψ' :

$$\psi' \equiv \frac{1}{\sqrt{\xi_F}} \frac{\lambda' - \tau'}{\sqrt{(1 + \lambda')\tau' + \kappa\sqrt{\tau'(\tau' + 1)}}}, \quad (8)$$

where $\tau' = \kappa^2 - \lambda'^2$. Also in the same model a small correction ($\propto \eta_F^2$),

$$\Delta = \xi_F(1 - \psi^2) \left[\frac{\sqrt{\tau(\tau + 1)}}{\kappa} + \frac{1}{3}\xi_F(1 - \psi^2)\frac{\tau}{\kappa^2} \right], \quad (9)$$

expresses (see Eqs. (4)) the impact of the medium on the single-nucleon electromagnetic cross section [17]. As far as the electric and magnetic form factors of the proton and the neutron G_{E_p}, G_{M_p} , G_{E_n} and G_{M_n} are concerned, we adopt the Höhler parametrization of Ref. [18].

Scaling of the first kind means that the function $F(\kappa, \psi)$ loses its dependence upon κ for large enough values of κ . To get rid as well of the dependence upon the momentum scale set by the nuclear structure itself, namely the Fermi momentum k_F , it is convenient to do as discussed in the Introduction and introduce a new dimensionless scaling function $f(\kappa, \psi)$ according to

$$f(\kappa, \psi) = k_F F(\kappa, \psi). \quad (10)$$

For the RFG one gets

$$f^{\text{RFG}}(\psi) = \frac{3}{4}(1 - \psi^2)\theta(1 - \psi^2), \quad (11)$$

namely, perfect superscaling. More generally Eq. (10) is the function upon which we shall focus to ascertain the superscaling properties of the QE response.

We shall carry out this task by comparing our predictions with the experimental $f(\kappa, \psi)$ extracted from the data of SLAC [19] and Jefferson Lab [20] (see Ref. [2] for a complete list of high-quality data in the relevant kinematic regions); that is, we compare the pure RFG response and the 2p-2h excitations induced by the MEC currents carried by the pion and the Δ with the data expressed in scaling form. As mentioned earlier, our computation will be confined to the 2p-2h transverse response function which for the RFG reads [9]:

$$\begin{aligned}
R_T(\mathbf{q}, \omega) = & \frac{1}{2} \frac{V}{(2\pi)^9} \int \frac{d\mathbf{p}_1 d\mathbf{p}_2 d\mathbf{p}'_1}{16 E_{\mathbf{p}'_1} E_{\mathbf{p}'_2} E_{\mathbf{p}_1} E_{\mathbf{p}_2}} \theta(|\mathbf{p}'_1| - k_F) \theta(|\mathbf{p}'_2| - k_F) \theta(k_f - |\mathbf{p}_1|) \theta(k_F - |\mathbf{p}_2|) \\
& \times \delta[\omega - (E_{\mathbf{p}'_1} + E_{\mathbf{p}'_2} - E_{\mathbf{p}_1} - E_{\mathbf{p}_2})] \sum_{\sigma\tau} \sum_{i,j=1}^3 V^4 \left(\delta_{ij} - \frac{q_i q_j}{\mathbf{q}^2} \right) \\
& \times \left[J_i^\dagger(\mathbf{p}'_1, \mathbf{p}_1, \mathbf{p}'_2, \mathbf{p}_2) J_j(\mathbf{p}'_1, \mathbf{p}_1, \mathbf{p}'_2, \mathbf{p}_2) \right. \\
& \quad \left. - J_i^\dagger(\mathbf{p}'_1, \mathbf{p}_1, \mathbf{p}'_2, \mathbf{p}_2) J_j(\mathbf{p}'_1, \mathbf{p}_2, \mathbf{p}'_2, \mathbf{p}_1) \right], \tag{12}
\end{aligned}$$

where the two terms in the last factor correspond to direct and exchange contributions. In Eq. (12) \mathbf{p}'_1 and \mathbf{p}'_2 (\mathbf{p}_1 and \mathbf{p}_2) are the three-momenta of the on-shell particles (holes) taking part in the process and $E_{\mathbf{p}} = \sqrt{\mathbf{p}^2 + m_N^2}$.

In Eq. (12) one needs the space components of the two-body MEC. As is well-known there are three of them, namely the pion-in-flight

$$\mathbf{J}_f^\mu(p'_1, p_1, p'_2, p_2) = -i \frac{1}{V^2} \frac{f_{\pi NN} f_{\gamma\pi\pi}}{\mu_\pi^2} (\boldsymbol{\tau}^{(1)} \times \boldsymbol{\tau}^{(2)})_3 \Pi(k_1)_{(1)} \Pi(k_2)_{(2)} (k_2 - k_1)^\mu, \tag{13a}$$

the seagull

$$\mathbf{J}_s^\mu(p'_1, p_1, p'_2, p_2) = -i \frac{1}{V^2} \frac{f_{\pi NN} f_{\gamma\pi NN}}{\mu_\pi^2} (\boldsymbol{\tau}^{(1)} \times \boldsymbol{\tau}^{(2)})_3 \left[\Pi(k_2)_{(2)} (\gamma^\mu \gamma^5)_{(1)} - \Pi(k_1)_{(1)} (\gamma^\mu \gamma^5)_{(2)} \right] \tag{13b}$$

and the Δ current (derived here using the Peccei Lagrangian)

$$\begin{aligned}
\mathbf{J}_\Delta^\mu(p'_1, p_1, p'_2, p_2) = & -\frac{1}{V^2} \frac{f_{\pi NN} f_{\pi N\Delta} f_{\gamma N\Delta}}{2m_N \mu_\pi^2} \left\{ \left[\left(\frac{2}{3} \tau_3^{(2)} - \frac{i}{3} (\boldsymbol{\tau}^{(1)} \times \boldsymbol{\tau}^{(2)})_3 \right) \left(j_{(a)}^\mu(p_a, k_2, q) \gamma_5 \right)_{(1)} \right. \right. \\
& + \left. \left. \left(\frac{2}{3} \tau_3^{(2)} + \frac{i}{3} (\boldsymbol{\tau}^{(1)} \times \boldsymbol{\tau}^{(2)})_3 \right) \left(\gamma_5 j_{(b)}^\mu(p_b, k_2, q) \right)_{(1)} \right] \Pi(k_2)_{(2)} + (1 \leftrightarrow 2) \right\}. \tag{13c}
\end{aligned}$$

In the above $k_1 = p'_1 - p_1$ and $k_2 = p'_2 - p_2$ are the momenta of the pions entering into each of the 2p-2h MEC diagrams (the four-momentum carried by the virtual photon is then $q = -k_1 - k_2$) and μ_π is the pion mass. Also one has

$$\Pi(k)_{(i)} = \frac{(\not{k} \gamma^5)_{(i)}}{k^2 - \mu_\pi^2}, \tag{14}$$

the index (i) distinguishing between the two interacting nucleons,

$$j_{(a)\mu}(p, k, q) = (4k_\beta - \not{k}\gamma_\beta)S^{\beta\gamma}(p, m_\Delta)\frac{1}{2}(-\gamma_\mu\not{q}\gamma_\gamma + q_\mu\gamma_\gamma) \quad (15a)$$

and

$$j_{(b)\mu}(p, k, q) = \frac{1}{2}(-\gamma_\beta\not{q}\gamma_\mu + q_\mu\gamma_\beta)S^{\beta\gamma}(p, m_\Delta)(4k_\gamma - \gamma_\gamma\not{k}), \quad (15b)$$

where $p_a \equiv p_1 - q$, $p_b \equiv p'_1 + q$, m_Δ is the Δ mass and $S^{\beta\gamma}$ the Rarita-Schwinger propagator. Finally, V is the volume enclosing our RFG.

We take $f_{\gamma\pi\pi} = 1$, $f_{\gamma\pi NN} = f_{\pi NN}$ and $f_{\pi NN}^2/4\pi = 0.08$ for the coupling constants in the Lagrangian. Although not explicitly indicated above, the currents are meant to include form factors, both hadronic and electromagnetic. For the former, in the present study we assume the standard monopole form

$$F_{\pi NN}(k^2) = \frac{\Lambda_\pi^2 - \mu_\pi^2}{\Lambda_\pi^2 - k^2}, \quad (16a)$$

$$F_{\pi N\Delta}(k^2) = \frac{\Lambda_{\pi N\Delta}^2}{\Lambda_{\pi N\Delta}^2 - k^2}, \quad (16b)$$

with $\Lambda_\pi = 1300$ MeV and $\Lambda_{\pi N\Delta} = 1150$ MeV, while for the latter we use the Höhler parameterization for the nucleon [18] and the expression [21]

$$F_{\gamma N\Delta}(q^2) = \frac{1}{(1 - q^2/\Lambda_D^2)^2} \left(1 - \frac{q^2}{\Lambda_2^2}\right)^{-\frac{1}{2}} \left(1 - \frac{q^2}{\Lambda_3^2}\right)^{-\frac{1}{2}} \quad (17)$$

for the $N \rightarrow \Delta$ transition form factor, with $\Lambda_D^2 = 0.71$ (GeV/c) 2 , $\Lambda_2 = M + M_\Delta$ and $\Lambda_3^2 = 3.5$ (GeV/c) 2 .

III. THE $\psi' < 0$ REGION

Even within the context of the RFG, the 2p-2h excitations induced by the MEC currents are nonzero throughout the entire spacelike region of the (κ, λ) plane. In contrast, within the RFG the 1p-1h contributions are confined to kinematics where $-1 \leq \psi \leq +1$, called the 1p-1h response region or Fermi cone. In this section we begin by presenting results in the $\psi' < 0$ region using the RFG for the 2p-2h MEC contributions in the scaling function f (referred to as f^{MEC}). We start by showing in Fig. 1 the interplay between first- and second-kind scaling by plotting f^{MEC} versus q for a few values of k_F , ranging from 50 to 300 MeV/c, at $\psi' = -2$, -1 and 0 . While, except for the lightest nuclei, k_F typically lies

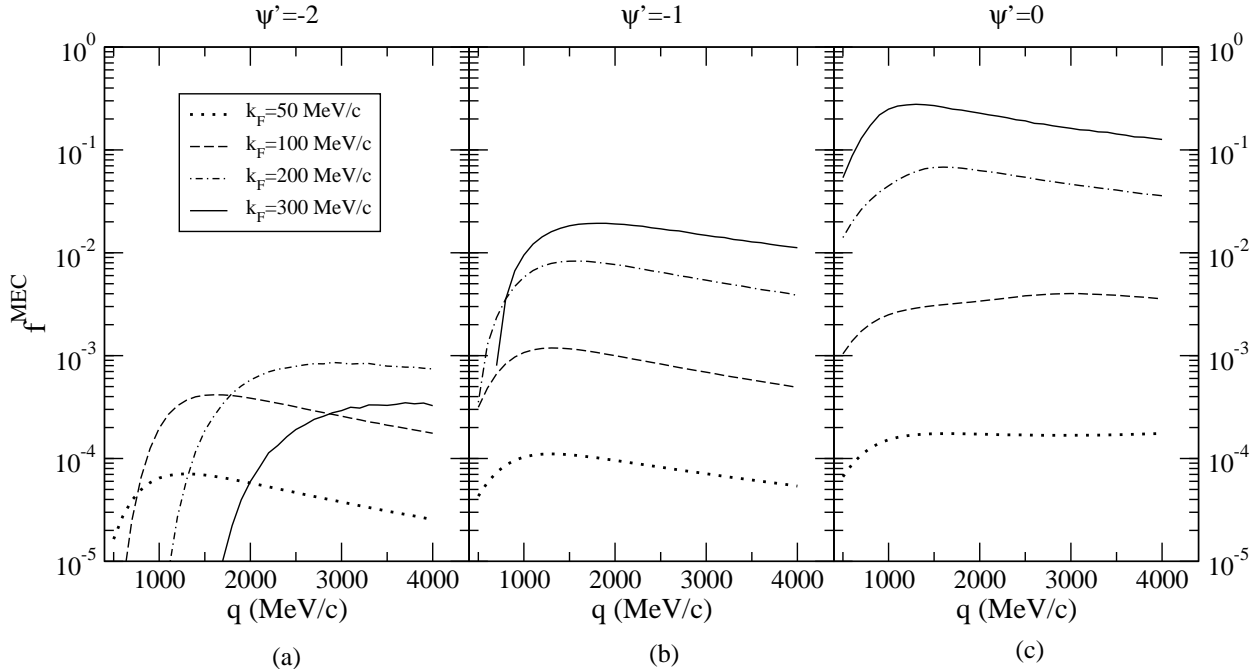


FIG. 1: MEC scaling function f^{MEC} versus q for three values of the scaling variable ψ' in the region below the QEP ($\psi' \leq 0$). The four types of curves correspond to four choices of k_F ranging from very small (few-body nuclei) to very large (beyond the heaviest nuclei studied).

in a much narrower range (200-250 MeV/c), we display results over this wider range to illustrate the trend better. In panel a of the figure ($\psi' = -2$) one observes that beyond some characteristic value of q lying roughly at 2-3 GeV/c first-kind scaling is seen to be well fulfilled for typical nuclei. As nuclei within the “typical nuclei range” become heavier (larger k_F) this onset is postponed to larger values of q . For $\psi' = -1$ (panel b), violations of first-kind scaling of f^{MEC} , although modest, are clearly apparent and persist for typical nuclei. A similar trend is seen for $\psi' = 0$ (panel c). Note, also, that very light nuclei (for example, deuterium has $k_F \approx 55$ MeV/c) would appear to have very little scaling violation in the QEP region, since the overall size of f^{MEC} is very minor compared with the usual one-body response for such small values of k_F .

In context we note that the additional contributions arising from 1p-1h MEC and correlation effects in the region of the QEP also need to be taken into account — in the RFG modeling this means in the region $-1 < \psi' < +1$. In Ref. [12] the net effect on the scaling behavior of these contributions was explored (see especially Fig. 7 of that reference) and, as here, scaling violations of both first and second kinds were predicted. The interference

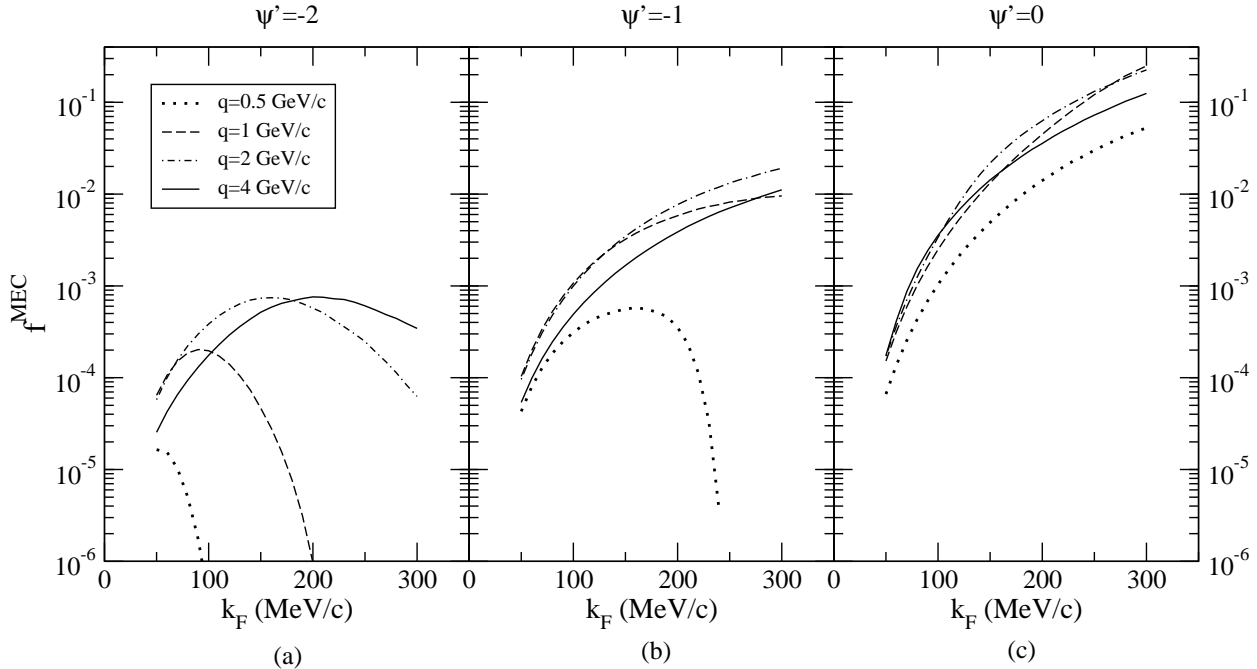


FIG. 2: As for Fig. 1, but now plotting the results as functions of k_F and with the curves shown corresponding to four choices for q .

between the one-body RFG contributions and these additional 1p-1h contributions reduces the cross section, typically by 10–15% in the QEP region for momentum transfers in the few GeV/c range, although there is a tendency towards restoration of scaling as q exceeds values around 2 GeV/c or so. At the values of q of interest in the present work scaling of the second-kind is broken roughly proportionally to k_F^3 and hence is relatively unimportant for very light nuclei, if not for medium-weight ones. For example, in going from carbon to gold (see below) at $q \approx 1$ GeV/c one finds a second-kind scale breaking of about 8% (see [12]).

In Fig. 2 we provide an alternative representation of the results displayed in Fig. 1, in order to address directly how the 2p-2h MEC contributions affect the issue of second-kind scaling. Here for $\psi' \leq 0$ we show f^{MEC} versus k_F for a few momentum transfers. Again, the figure clearly conveys the information that f^{MEC} generally has significant dependence on k_F , i.e., does not show scaling behavior of the second kind. For typical nuclei a range of kinematics can be found where the curves are relatively flat; however, for most choices of kinematics a strong k_F -dependence is observed. For example, in the region of the QEP at high q the curves shown in the figure go roughly as k_F^3 except where k_F is very small.

Note that the behavior found in Fig. 2 at negative values of ψ' — namely that f^{MEC}

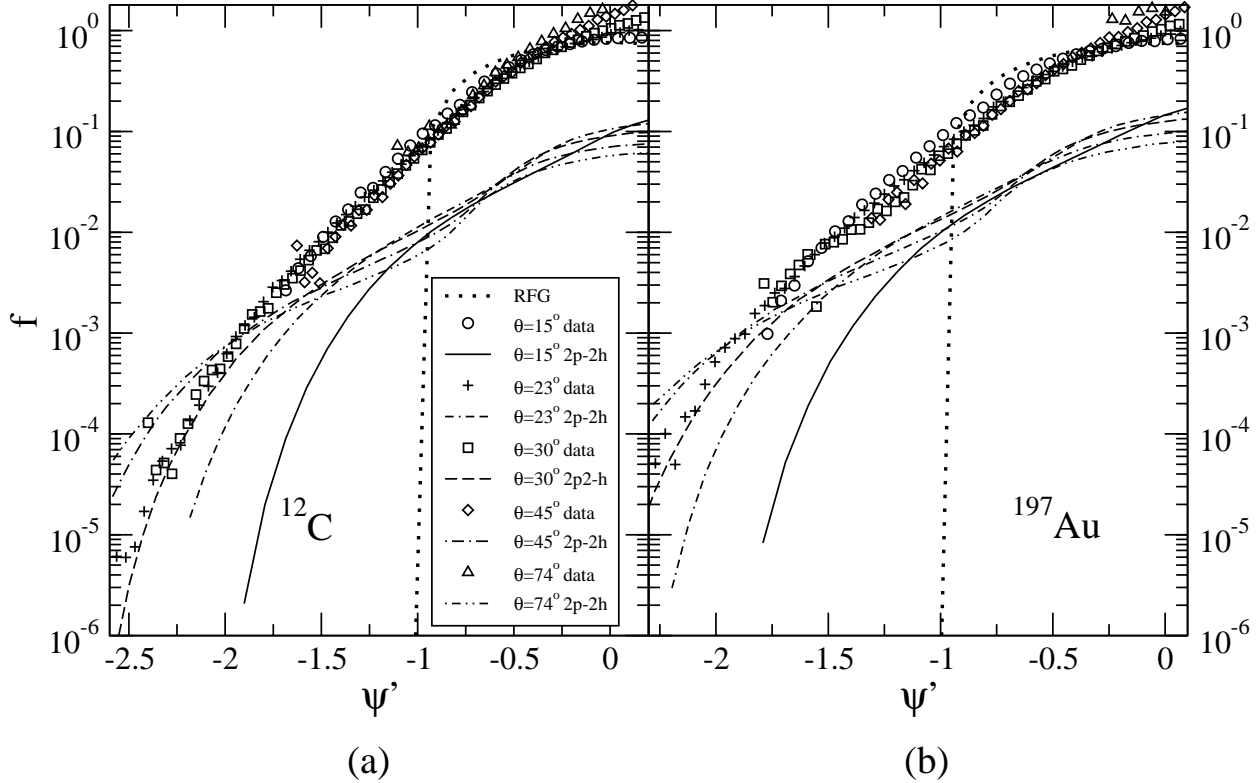


FIG. 3: The dimensionless scaling function f plotted versus the scaling variable ψ' for JLab data [20] using carbon (panel a) and gold (panel b) targets with electrons of 4045 MeV and the scattering angles given in the legend. The legend also labels the curves showing f^{MEC} computed as discussed in the text.

reaches a maximum and then decreases with a pronounced q -dependence — is just a consequence of the particular kinematical conditions found in this domain. In fact, at fixed q in the range relevant in the present work and negative ψ' , when k_F grows one is actually probing the nuclear response function at lower and lower transferred energy λ (or ω). This can be easily checked by rendering explicit the dependence of λ on ψ' via Eq. (8) and by imposing the physical requirement $\lambda > 0$: one then finds an upper bound on k_F , specifically, $\eta_F \lesssim -\kappa/\psi'$.

Next we turn to comparisons of our results with existing high- q data. We start by displaying and comparing our results with the data obtained at JLab [20] for ^{12}C in Fig. 3a and ^{197}Au in Fig. 3b. The data shown in the figure were taken with an electron beam energy of 4045 MeV, scattered at angles of $\theta = 15^\circ, 23^\circ, 30^\circ, 45^\circ$ and 74° . Note that the momentum transfer q depends not only on the beam energy and scattering angle, but also on the energy

being transferred and therefore on ψ' : for the energy transfers spanned by the experiment, these values of the scattering angle roughly correspond to three-momentum transfers in the ranges 1–1.4, 1.6–1.8, 2–2.4, 2.9–3.1 and 3.9 GeV/c, respectively. Since in this figure we restrict our attention to the left of the QEP, the actual variation in momentum transfer is small and, for the sake of the discussion, one can just consider the lower limits in the above ranges. As far as the modeling is concerned, from previous studies [3] we know to ascribe a k_F of 228 (245) MeV/c and an energy shift of 20 (25) MeV to carbon (gold).

Comparisons with the data must be made carefully: each data set with a given scattering angle (and therefore roughly a given value of q , as noted above) extends down only to a specific value of ψ' . In particular, for $\theta = 15^\circ, 23^\circ, 30^\circ, 45^\circ$ and 74° , for carbon (panel a in the figure) these values are $\psi'_{min} \approx -1.7, -2.6, -2.4, -1.6$ and -1.1 , respectively. For gold (panel b) the corresponding numbers are $\psi'_{min} \approx -1.8, -2.3, -1.7, -1.3$ and -1.3 , respectively. This is made clearer in Fig. 4 where the ratio of the JLab data f^{\exp} given in Fig. 3 to the calculated f^{MEC} is shown both for carbon (panel a) and gold (panel b). Clearly one sees from this representation that typically the size of the MEC contributions is 10% or less (i.e., the ratio in Fig. 4 is 10 or larger), except at large negative values of ψ' . Such conditions can be met by these data sets only for $\theta = 23^\circ$ and 30° , and in the latter case really only for carbon, as the 30° gold data do not extend below about -1.7 . In the discussions to follow, this will limit the most stringent test of second-kind scaling to the 23° case.

Let us begin the comparisons of f^{MEC} with the data in the negative ψ' region by addressing the issue of *scaling of the first kind*, namely the behavior of f versus ψ' as the momentum transfer q is varied. From Fig. 3 one sees that outside of the Fermi cone the 2p-2h scaling function is small at low momentum transfers (forward angles) and then grows with q . For a specific choice of ψ' there appears to be a characteristic value of q at which the first-kind scaling behavior sets in (see also Fig. 1 above). For example, if one fixes one's attention to $\psi' = -2$, this stabilization occurs for q a little larger than 2 GeV/c. Ideally, comparisons would be made with the data for a wide range of momentum transfers at large negative ψ' (say, below -2) where the 2p-2h MEC effects are predicted to be relatively large and thereby would see the approach to first-kind scaling. However, as is made clear by Fig. 4, for very large q the range in ψ' is relatively narrow and only the 23° and 30° data extend below $\psi' = -2$, and there only for carbon. In this region of kinematics to test high- q , low- ψ'

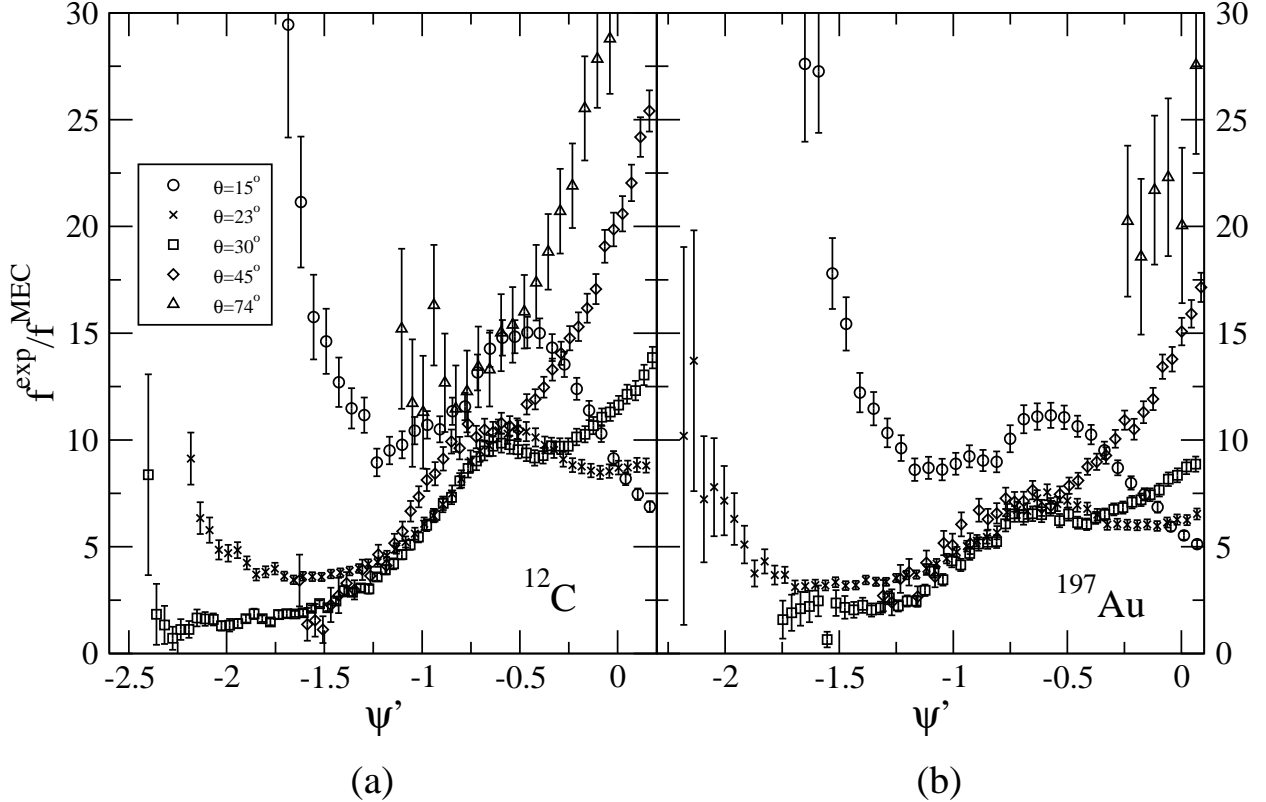


FIG. 4: Ratio of the JLab data f^{exp} shown in Fig. 3 to the calculated f^{MEC} both for carbon (panel a) and gold (panel b).

first-kind scaling behavior one therefore has only the carbon data for $\theta = 23^\circ$ where, as noted above, $q \approx 1.6 \text{ GeV}/c$ and for $\theta = 30^\circ$ where $q \approx 2 \text{ GeV}/c$. From the figures one sees that the amount of scaling violation provided by the 2p-2h MEC contributions is clearly compatible with the scaling violations seen in the data. At less negative values of ψ' the ratios presented in Fig. 4 show that the relative size of f^{MEC} is typically only about 10% or less of the full f and that the first-kind scaling violations, even at the highest values of q , are again compatible with the amount seen in the data.

As discussed above, note that inside the Fermi cone, where the 2p-2h MEC provide roughly a 10% contribution, other competing effects must also be taken into account. In particular, it is known that the 1p-1h MEC and correlation contributions must be considered. These interfere with the one-body contributions — the basic RFG contributions — and so decrease the scaling function from its RFG value in this domain by roughly the same amount as the 2p-2h MEC provide as additions [10, 11, 12]. Since the 1p-1h and 2p-2h response functions add incoherently, one expects them to cancel each other to a large extent in the

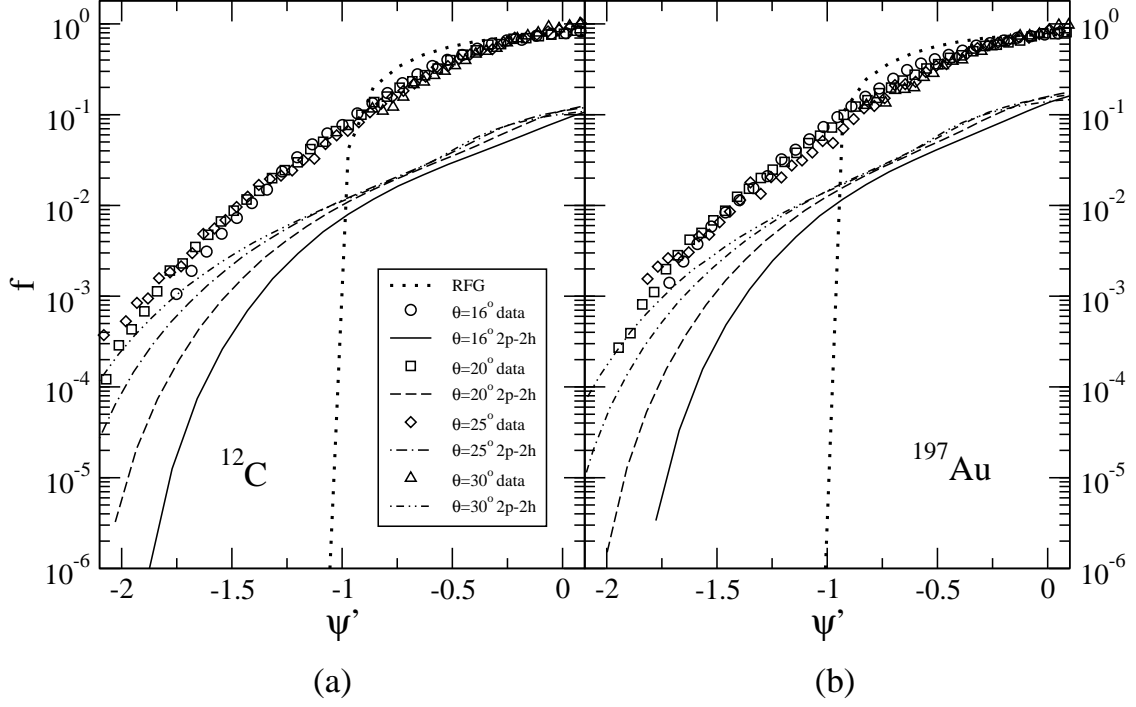


FIG. 5: As for Fig. 3, but now for SLAC data [19] taken at 3595 MeV for the angles listed in the legend. The curves are as in Fig. 3.

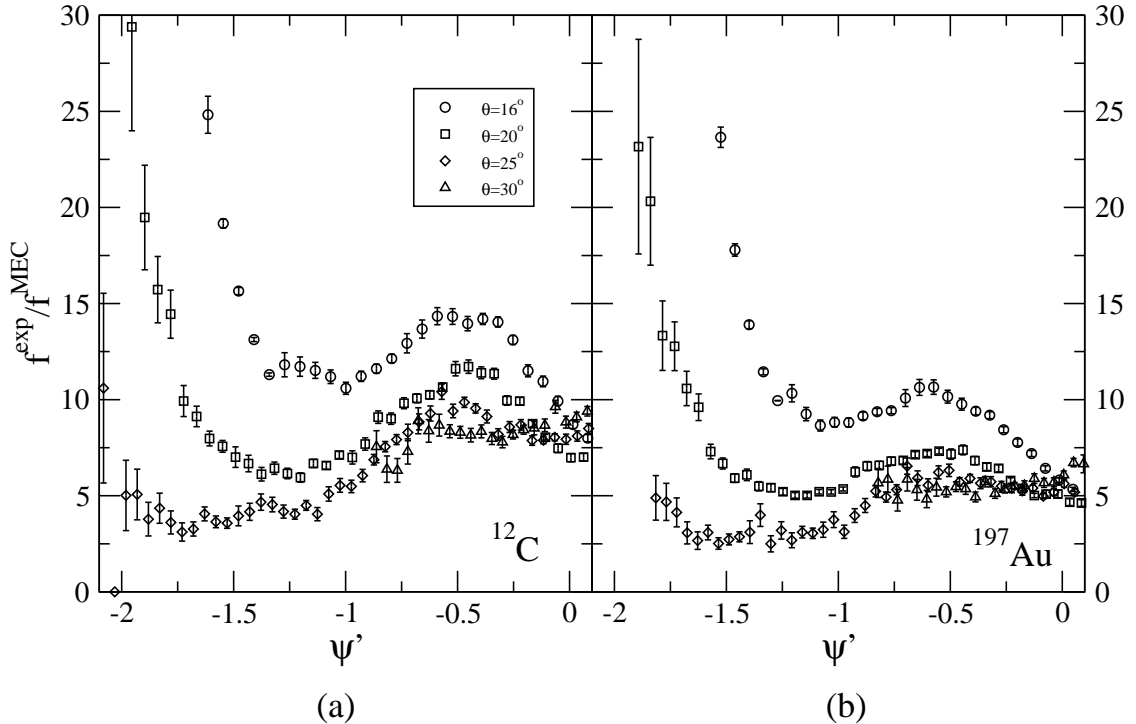


FIG. 6: Ratio of the SLAC data f^{exp} shown in Fig. 5 to the calculated f^{MEC} both for carbon (panel a) and gold (panel b).

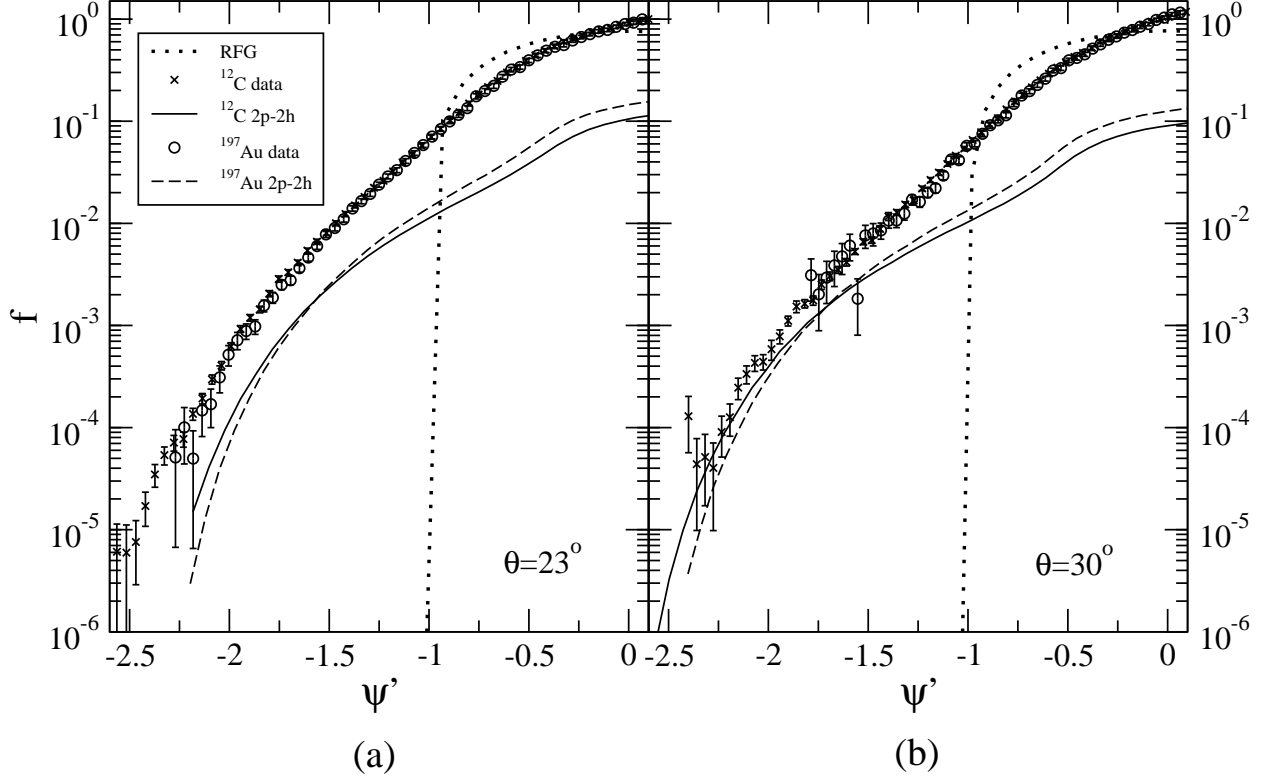


FIG. 7: The dimensionless scaling function f plotted versus the scaling variable ψ' for JLab data [20] at $\theta = 23^\circ$ (panel a) and 30° (panel b), as well as the results obtained for f^{MEC} for carbon (crosses and solid curve) and gold (circles and dashed curve).

QEP region.

For the sake of completeness, in Figs. 5 and 6 we display the scaling function f^{MEC} for ^{12}C and ^{197}Au as in Figs. 3 and 4, but now here for data from SLAC [19] taken with a beam of energy 3595 MeV and scattering angles $\theta = 16^\circ, 20^\circ, 25^\circ$ and 30° . Accordingly, the associated momentum transfers probed in these experiments now span the ranges 1–1.7, 1.2–1.4, 1.5–1.7 and 1.9–2.4 GeV/c, respectively. Again, the actual momentum range probed in the negative- ψ' region is smaller, and the lower limits may be taken as typical values. The minimum values attained for the scaling variable are, for carbon $\psi'_{\min} \approx -1.8, -2.1, -2.1$ and -0.9 , and for gold $\psi'_{\min} \approx -1.7, -2.0, -1.8$ and -0.8 , for the above set of angles, respectively. The results observed are rather similar to those presented in Figs. 3 and 4.

Let us next discuss the *second-kind scaling* behavior seen at large negative ψ' . In fact, as the above figures show, the only cases where both carbon and gold data extend down to this region are those for $\theta = 23^\circ$ and 30° . Accordingly, in Fig. 7 the JLab data for $\theta = 23^\circ$

(panel a) and 30° (panel b) are separated out from Fig. 3 and again compared with f^{MEC} , but now simultaneously for carbon (crosses and solid curve) and gold (circles and dashed curve). Starting with the 23° case shown in Fig. 7a, one observes the following: at the QEP ($\psi' = 0$) one finds that f^{MEC} is about 13% of the experimental f and that the second-kind scaling violation implied by the difference between the curves for carbon and gold amounts to about 4%. As already noted above, the results shown here do not take into account the 1p-1h MEC + correlation contributions which decrease the overall non-impulse-approximation effect, making these numbers over-estimates. Both classes of contributions go roughly as k_F^3 at high q and so the partial cancellation is relatively independent of the actual species of nuclei being examined.

In contrast, at large negative ψ' the only scale-breaking contributions in the present model are those provided by the 2p-2h MEC terms and, in fact, on the one hand we see that they can have relatively large effects when compared with the full experimental scaling function — for instance, at $\psi' = -2$ one finds that f^{MEC} is about 16% of the experimental f . On the other hand, the second-kind scaling violation implied by the difference between the curves for carbon and gold amounts to about 7% for these kinematics, interestingly with the gold curve lying below that for carbon, in contrast to the behavior above $\psi' \approx -1.6$ where the reverse is true. Thus, for the high- q , large-negative- ψ' region covered by the 23° data for carbon and gold one sees some violation of scaling of the second kind, although such MEC effects alone appear not to destroy the excellent scaling seen in the existing data. Indeed, slight adjustments in the choices of k_F and E_{shift} can be made (these are, after all, empirically determined [3]) and thereby can also provide changes of this size. However, as shown in Fig. 7b where results at 30° and hence large q are shown, it does not take too much for the MEC effects, including the amount of second-kind scale breaking they provide, to become significant. Unfortunately, as noted above, the gold data do not extend down to very low values of ψ' for these conditions and so it is not presently possible to see clear evidence for such contributions. Finally, we note that for intermediate negative values of ψ' the net degree of second-kind scale-breaking is expected to be only a few percent and clearly compatible with what is seen in the data.

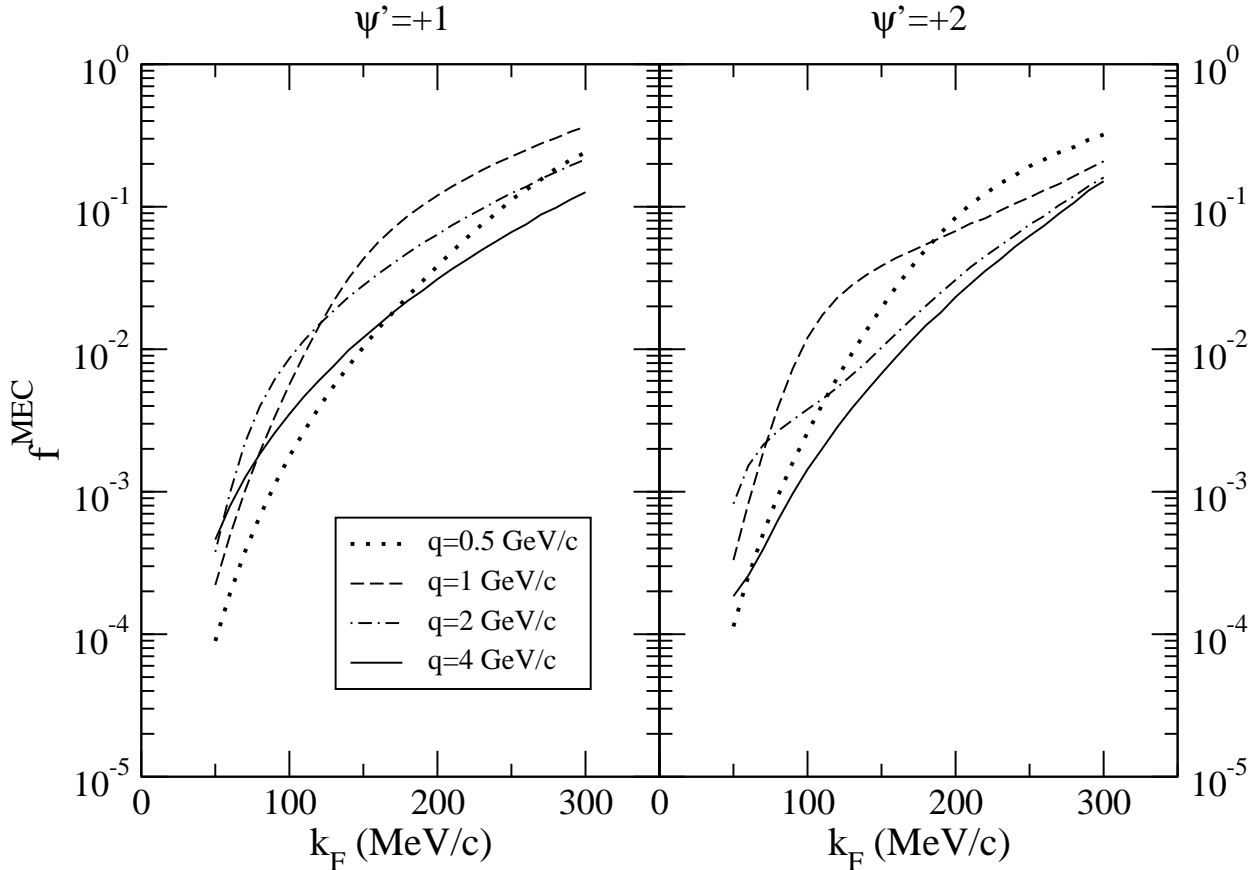


FIG. 8: As for Fig. 2, but now for the region above the QEP.

IV. THE $\psi' > 0$ REGION

In the region $\psi' > 0$ at sufficiently high q baryon resonances, meson production and eventually deep inelastic scattering (DIS) make significant, even dominant, contributions to the total response. This regime has recently been explored in Ref. [16] in which an *inelastic* version of the basic RFG approach, together with an extension called the ERFG, were studied (the reader is directed to the cited reference for details). Additionally, here we also have contributions from f^{MEC} .

To explore how f^{MEC} may or may not violate second-kind scaling in the domain $\psi' > 0$, as in the previous section we begin by showing results versus k_F in Fig. 8 at $\psi' = 1$ and 2. Here it is quite apparent that the 2p-2h MEC excitations alone substantially break the second-kind scaling. For example, at $\psi' = 1$ in going from ^{12}C to ^{197}Au there is roughly a 20% increase in f^{MEC} at $q = 1 \text{ GeV/c}$ and a 35% increase at $q = 4 \text{ GeV/c}$.

Furthermore, the 2p-2h MEC contributions that arise from the modeling discussed in the

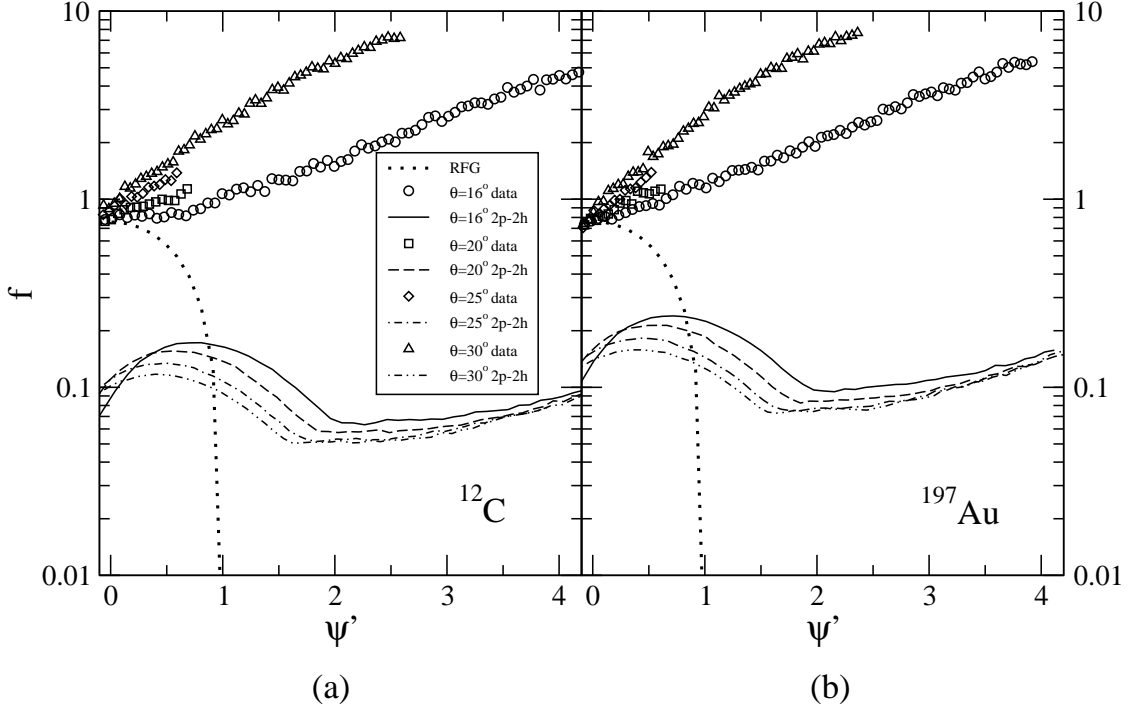


FIG. 9: As for Fig. 5, showing data from SLAC [19] and results for f^{MEC} , but now for the region above the QEP ($\psi' \geq 0$).

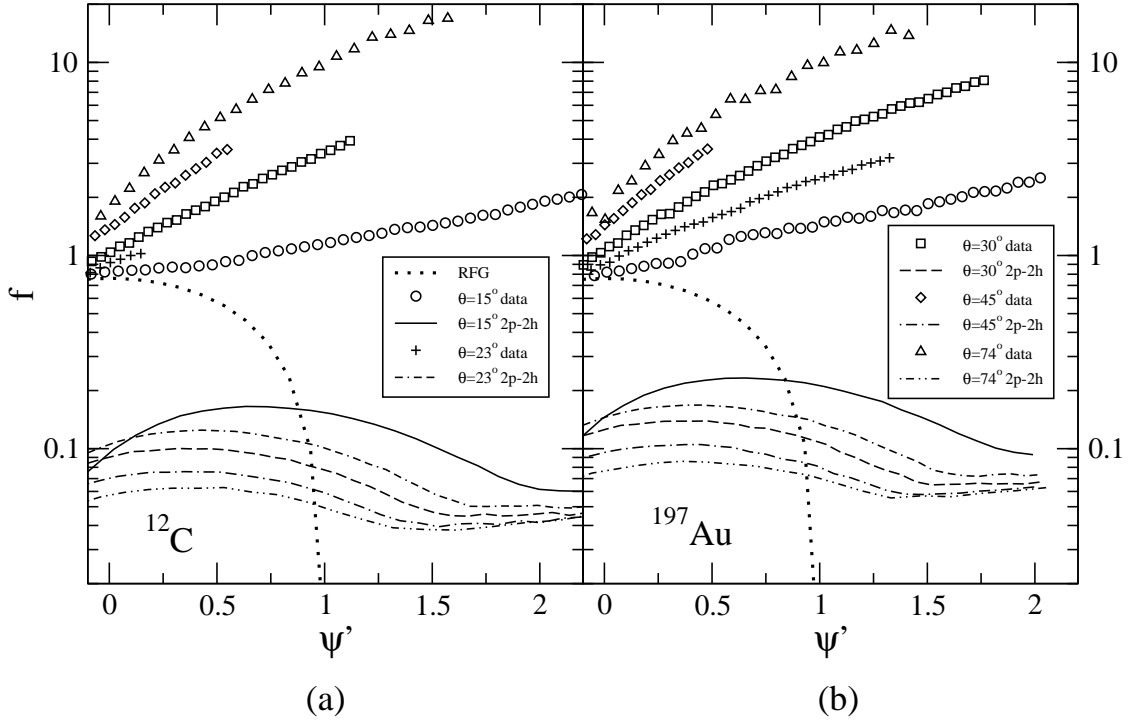


FIG. 10: As for Fig. 9, but now showing comparisons with data from JLab [20].

present work can provide significant contributions to the total scaling function, especially at lower values of q . To get a feeling for the size of these when ψ' is positive, we display f^{MEC} together with f^{RFG} in Fig. 9 (where the SLAC data are also shown) and in Fig. 10 (where the JLab data are displayed), again for ^{12}C and ^{197}Au . In the figures it is seen that f^{MEC} is significant around $\psi' = 1$, accounting for roughly 10–20% of the data for q below 2 GeV/c, down to a few percent at the highest momenta. Note that the trend is in the right direction: the heavier nucleus (larger k_F) has a larger 2p-2h MEC contribution than does the lighter one, in concert with what is observed in the data.

Putting these two pieces of information together we see that the degree of second-kind scaling violation that arises from the 2p-2h MEC contributions obtained in the present work is a few percent at modest q , dropping to the sub-one-percent level at higher q . This is smaller than the amount found in Ref. [3], namely that in the domain $\psi' > 0$ second-kind scaling in the total scaling function f is violated at about the 20% level. There it was observed that the inelasticity mentioned above itself violates scaling of the second kind and clearly dominates the total inclusive cross section. The follow-up study in Ref. [16] makes this point even clearer (see, for example, Fig. 12 in that reference where the $\theta = 16^\circ$ SLAC data also shown in Fig. 9 are compared with the inelastic RFG and ERFG model results). Thus, at least at the point reached in addressing the nature of the inclusive cross section in the region above the QEP, we find that, while the 2p-2h MEC effects can be important at modest values of q , they do not apparently break the second-kind scaling behavior by more than a few percent and that the actual scale-breaking observed comes from other effects.

A final thing to note is that the 2p-2h MEC contributions violate first-kind scaling in the opposite direction to the trend displayed by the data, since one observes a decreasing of f^{MEC} with increasing q . This is also opposite to the behavior seen in the scale-breaking seen in the inelastic modeling reported in Ref. [16], which behaves more the way the data do. At higher values of ψ' , f^{MEC} stays relatively constant, whereas the data definitely grow, the more so the higher the value of q .

V. ROLE OF THE Δ

Δ -dominance in both the 1p-1h and 2p-2h sectors of the RFG Hilbert space has been plainly demonstrated in Refs. [10] and [9], respectively. As we shall see, this comes about

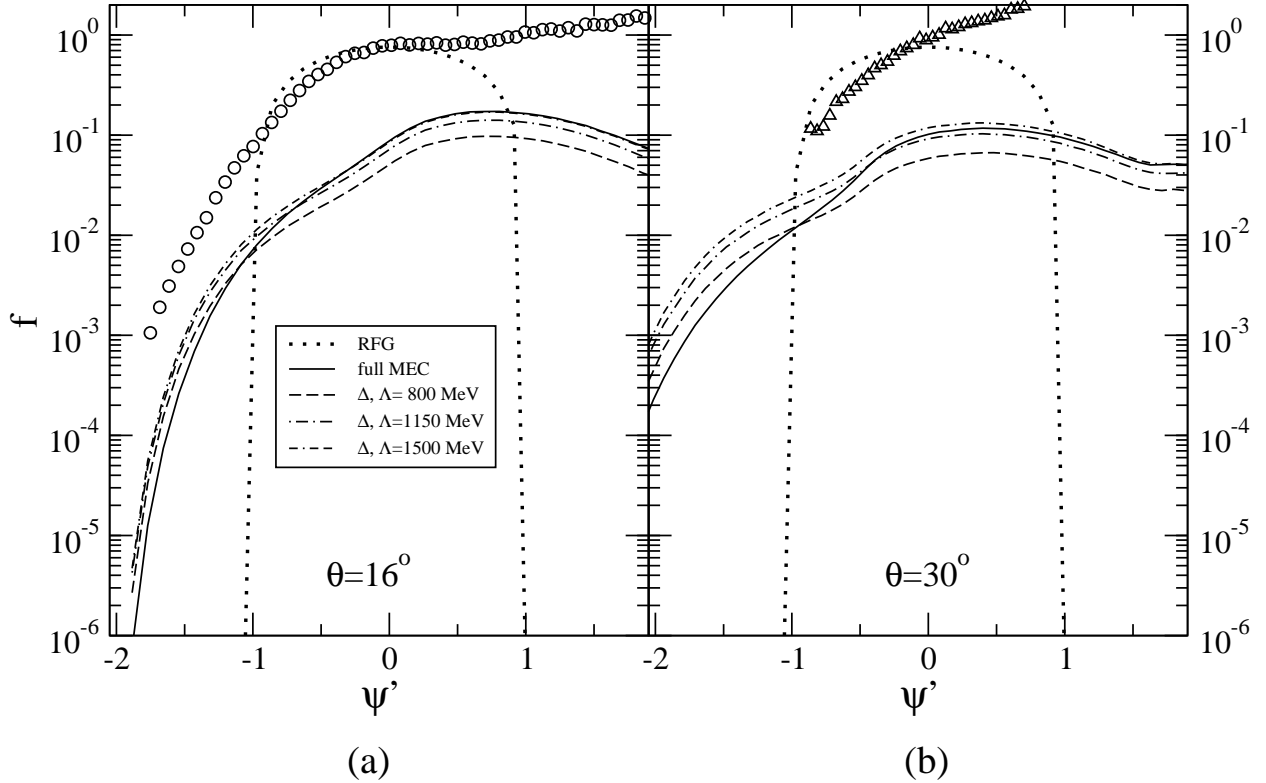


FIG. 11: The scaling function for ^{12}C at the kinematics of the experiments of Ref. [19] for $\theta = 16^\circ$ (a) and 30° (b). The dotted line represents f^{RFG} and the solid line f^{MEC} in the full model, whereas all the other curves represent f^{MEC} including only the Δ -current for different choices of the strong $\pi N \Delta$ cutoff, $\Lambda_{\pi N \Delta}$ (abbreviated to Λ here). Results are shown for $\Lambda = 800$ MeV (dash), 1150 MeV (dot-dash) and 1500 MeV (dot-dash-dot). As usual, for carbon one has $k_F = 228$ MeV/c and $E_{\text{shift}} = 20$ MeV.

through a rather delicate cancellation, and accordingly we shall explore in a bit more depth two aspects of these issues. On the one hand, we wish to investigate the sensitivity of the contributions made by the Δ -current to the 2p-2h excitations with respect to variations of the poorest-known parameter entering into the definition of the Δ -current itself, namely, the cutoff in the hadronic form factor in Eq. (16b). On the other hand, we wish to gauge the relative role played by the Δ via comparisons of the 2p-2h MEC contribution computed using the whole set of MEC in Eqs. (13) with those arising from the Δ alone.

In Fig. 11 the basic RFG scaling function and f^{MEC} are displayed, together with the SLAC data taken at $\theta = 16^\circ$ (panel a) and $\theta = 30^\circ$ (panel b), versus ψ' for ^{12}C . The 2p-2h MEC scaling function is computed in the full model and with the Δ alone, in the latter case

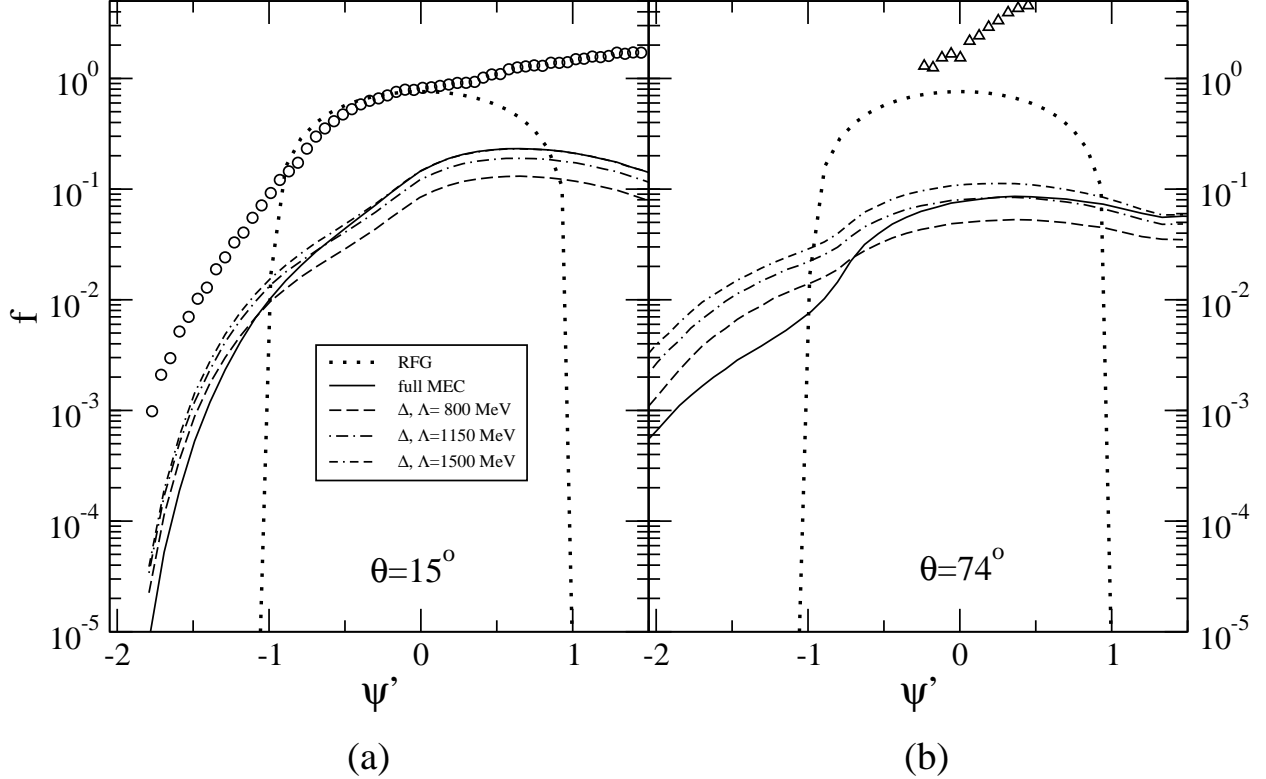


FIG. 12: As in Fig. 11, but for ^{197}Au at the kinematics of the experiments of Ref. [20] for $\theta = 15^\circ$ (a) and 74° (b); $k_F = 245$ MeV/c and $E_{\text{shift}} = 25$ MeV.

in three different versions, corresponding to three values of the cutoff in Eq. (16b), namely $\Lambda_{\pi N \Delta} = 800, 1150$ and 1500 MeV. The same analysis is carried out for ^{197}Au and presented in Fig. 12, now with the JLab data at $\theta = 15^\circ$ (panel a) and $\theta = 74^\circ$ (panel b). Interesting features emerge from the two figures.

First, concerning ^{12}C , we recall the discussions of kinematics made earlier: in panel (a) one has $1 \lesssim q \lesssim 1.7$ GeV/c, whereas in panel (b) one has $1.9 \lesssim q \lesssim 2.4$ GeV/c. For these ranges of three-momentum transfer it is observed that within the Fermi cone the non- Δ terms (those arising from diagrams having only nucleons and pions) play quite a minor role, almost insignificant at small q , and that the harder the $\pi N \Delta$ vertex, the larger the Δ contribution. In contrast, in the scaling region ($\psi' \lesssim -1$), it turns out that the Δ by itself yields a contribution that is substantially larger than the one found with the full MEC and that this becomes more pronounced as q grows.

This behavior, in fact, stems from the interferences between the Δ and non- Δ contributions which are of opposite sign [9]. That is, we see that the non- Δ currents, while giving

rise to small contributions in themselves, actually open the door to significant interference effects. This is emphasized in Fig. 12, where the MEC are probed at substantially larger momenta, namely $q \approx 3.9$ GeV/c in panel (b).

VI. DISCUSSION AND CONCLUSIONS

The concept of scaling is based on having some basic “elementary” cross section for scattering from the constituents in a system which can reasonably be factored out, leaving a reduced cross section whose nature is determined essentially by the distribution of the constituents. Given that a decomposition of this sort is indeed reasonable, that is, that a factorization of this type occurs at least for the dominant contributions in the cross section (coherent scatterings, for example, would not tend to have such a property), it is often the case that the reduced cross section is in fact a relatively universal function of one or more scaling variables, namely, that the results scale and one has a very compact representation of the cross section [1]. This is certainly true when the constituents of the system are “simple” or behave as such, as happens for the partons in the nucleon (asymptotic freedom) or for the electrons in an atom at appropriate energies. However, it can remain true even when the constituents are complex, as for atoms in solids and, as the studies discussed in the present work indicate, for nuclei at high q and excitations spanning a wide range from below the quasielastic peak through the resonance region and into the regime where DIS is beginning to become applicable. On the other hand, it is certainly not a valid way to proceed in all circumstances; for instance, very near threshold in electroexcitation one has collectivity and the factorization is clearly broken.

Even in the kinematical region where the dominant contribution appears to scale, one knows that other processes can also play some role and therefore that several questions arise. Do such additional contributions show either first- or second-kind scaling behaviors or not? If not, are they sizable contributions relative to the dominant (scaling) processes, and therefore, if they do not scale, is the modeling in conflict with observation or not? Or, said another way, how much scaling violation is to be expected from these additional contributions?

In the present context, where we are focusing on the scaling, QEP and resonance regions for inclusive electron scattering at high q , one can think of several physical processes of this

type that might provide some degree of scale-breaking beyond the basic impulsive process (the RFG model in the present work) which does have the scaling properties. In particular, we know from work already done [10, 11, 12] that MEC effects and correlations in the 1p-1h sector do not in general have scaling of either the first or second kind, although the degree of scale-breaking is relatively small under most circumstances. Moreover, in the resonance region and beyond we know that inelastic, but impulsive scattering from nucleons in the nucleus also breaks both kinds of scaling [3, 16], and in a way that tends to improve the agreement with the data (which also do not scale in that region).

Still other effects remain to be explored. In particular, it would be highly desirable to have relativistic treatments of correlation effects not just for the 1p-1h sector alluded to above, but also in the 2p-2h sector, since these are known to be sizable at least in non-relativistic calculations at low momenta [22]; one would like relativistic modeling of short-range NN correlations as well, as they are expected to contribute especially in the large-negative- ψ' region [23]; furthermore, additional many-body interaction effects (such as via RPA correlations) may play a role; and nuclear binding effects arising, for example, in a relativized shell model approach should also be explored. Most of these are presently being revisited in a relativistic context in other on-going work.

In the present work we have considered one other specific process which naturally does not scale, namely, the effects arising from 2p-2h MEC contributions. We employ currents arising both from diagrams containing the Δ and those built only from nucleons and pions (non- Δ terms), and in a brief section present results to show the delicate interplay between these two classes of diagrams and to indicate the cutoff-dependence in the former. Our present studies are based on recent work [9] where these pieces of the cross section were derived and comparisons were made with other existing studies.

Our motivation for the present work is a specific one: here we have focused on the scaling properties of the 2p-2h MEC contributions. Results are presented for kinematics ranging from far below the QEP (at large negative ψ'), in the region of the QEP (near $\psi' = 0$) and beyond (at positive ψ') where resonances and DIS can both play significant roles. We have found that scaling of both the first and second kinds is generally broken by these contributions.

At large negative ψ' we have seen a stabilization with increasing q at fixed ψ' set in, so that at very high values of q the first-kind scaling behavior appears to be recovered. On

the other hand, also at large negative ψ' , we see violations of second-kind scaling that are compatible with the existing data in this region; however, the results obtained here suggest that, were data on several nuclei to become available at still higher values of q , one might begin to see significant second-kind scaling violations.

In the vicinity of the QEP ($-1 < \psi' < +1$) we have continued to see a delicate interplay between the MEC+correlation effects in the 1p-1h sector and the present 2p-2h MEC effects — the former interfere with the impulsive RFG response and lead to a decrease in the net 1p-1h result, whereas the 2p-2h MEC effects go in the opposite direction and tend to restore the final total answer back to where one began.

In the large-positive- ψ' region we find that the second-kind scaling is again violated, but not by very much compared with the data. Indeed, it is clear from previous work that the main scaling violations in this regime stem from the inelastic, but impulsive excitations. This is not to say that the 2p-2h MEC contributions are insignificant — they account for perhaps 10–20% of the total strength in the resonance region — just that they appear to provide only few percent violations of second-kind scaling. Interestingly, in this region the first-kind scaling is also violated by the 2p-2h MEC contributions, but with a trend that is opposite to what is observed in the data and also in the inelastic modeling.

VII. ACKNOWLEDGMENTS

This work has been supported in part by the INFN-MIT Bruno Rossi Exchange Program and by MURST (contract No. 2001024324_007) and in part (TWD) by funds provided by the U.S. Department of Energy under cooperative research agreement No. DE-FC02-94ER40818.

- [1] T.W. Donnelly and I. Sick, Phys. Rev. Lett. **82** (1999) 3212.
- [2] T.W. Donnelly and I. Sick, Phys. Rev. **C60** (1999) 065502.
- [3] C. Maieron, T.W. Donnelly and I. Sick, Phys. Rev. **C65** (2002) 025502.
- [4] W.M. Alberico, A. Molinari, T.W. Donnelly, L. Kronenberg and J.W. Van Orden, Phys. Rev. **C38** (1988) 1801.
- [5] M.B. Barbaro, R. Cenni, A. De Pace, T.W. Donnelly and A. Molinari, Nucl. Phys. **A643** (1998) 137.

- [6] R. Cenni, T.W. Donnelly and A. Molinari, Phys. Rev. **C56** (1997) 276.
- [7] J. Jourdan, Nucl. Phys. **A603** (1996) 117.
- [8] W.M. Alberico, A. Molinari and T.W. Donnelly, Nucl. Phys. **A512** (1990) 541.
- [9] A. De Pace, M. Nardi, W.M. Alberico, T.W. Donnelly, and A. Molinari, Nucl. Phys. **A276** (2003) 303.
- [10] J.E. Amaro, M.B. Barbaro, J.A. Caballero, T.W. Donnelly and A. Molinari, Phys. Rep. **368** (2002) 317.
- [11] J.E. Amaro, M.B. Barbaro, J.A. Caballero, T.W. Donnelly and A. Molinari, Nucl. Phys. **A697** (2002) 388.
- [12] J.E. Amaro, M.B. Barbaro, J.A. Caballero, T.W. Donnelly and A. Molinari, Nucl. Phys. **A723** (2003) 181.
- [13] J.E. Amaro, G. C  , E.M.V. Fasanelli and A.M. Lallena, Phys. Lett. **B277** (1992) 249.
- [14] J.E. Amaro, G. C   and A.M. Lallena, Ann. Phys. (N.Y.) **221** (1993) 306.
- [15] J.E. Amaro, G. C   and A.M. Lallena, Nucl. Phys. **A365** (1994) 365.
- [16] M.B. Barbaro, J.A. Caballero, T.W. Donnelly and C. Maieron (to be published in Phys. Rev. C, nucl-th/0311088).
- [17] P. Amore, R. Cenni, T.W. Donnelly and A. Molinari, Nucl. Phys. **A615** (1997) 353.
- [18] G.H  hler, E. Pietarinen, I. Sabba-Stefanescu, F. Borkowski, G.G. Simon, V.H. Walther and R.D. Wendling, Nucl. Phys. **B114** (1976) 505.
- [19] D.B. Day *et al.*, Phys. Rev. **C48** (1993) 1849.
- [20] J. Arrington *et al.*, Phys. Rev. Lett. **82** (1999) 2056.
- [21] M.J. Dekker, P.J. Brussaard and J.A. Tjon, Phys. Rev. **C49** (1994) 2650.
- [22] W.M. Alberico, M. Ericson, and A. Molinari, Ann. Phys. (N.Y.) **154** (1984) 356.
- [23] O. Benhar, A. Fabrocini, S. Fantoni and I. Sick, Nucl. Phys. **A579** (1994) 493.